Hindawi
Advances in Civil Engineering
Volume 2020, Article ID 2847027, 17 pages
https://doi.org/10.1155/2020/2847027

Research Article

FRP Composite in Mitigating Seismic Risk of RC Structures in Near-Fault Regions with/without Aftershocks

Vui Van Cao [1,2] **and Son Quang Pham** [1,2]

[1] *Faculty of Civil Engineering, Ho Chi Minh City University of Technology (HCMUT), 268 Ly Thuong Kiet Street, District 10, Ho Chi Minh City, Vietnam*
[2] *Vietnam National University-Ho Chi Minh City (VNU-HCM), Linh Trung Ward, Thu Duc District, Ho Chi Minh City, Vietnam*

Correspondence should be addressed to Vui Van Cao; cvvui@hcmut.edu.vn

Received 29 November 2019; Revised 31 May 2020; Accepted 10 June 2020; Published 8 July 2020

Academic Editor: John Mander

The literature related to earthquakes and fibre reinforced polymer (FRP) retrofitting can be divided into two main categories: (1) the applications of FRP to retrofit structures subjected to single traditional earthquakes and (2) the effects of mainshock-aftershock sequences on original structures (without FRP retrofitting). Research on using FRP to mitigate the risk of pulse-type mainshock-aftershock sequences for reinforced concrete (RC) structures located in near-fault regions is hardly found in the literature and is thus the aim of this study. To achieve this aim, a four-storey RC frame, near-fault mainshocks, and seismic sequences were selected. The frame was retrofitted using FRP wraps at plastic hinge locations. Nonlinear time history and damage analyses of the original and FRP-retrofitted frames subjected to these near-fault mainshocks and seismic sequences were conducted. The results showed that aftershocks significantly increase the damage indices of the frames, shifting the damage state of the original frame from severe damage to collapse and the damage state of the FRP-retrofitted frame from light damage to moderate damage. FRP retrofitting successfully reduced the risk of seismic sequences by reducing the damage two levels, shifting the damage state of the original frame from collapse to moderate damage.

1. Introduction

The majority of strong earthquakes are commonly followed by aftershocks [1] as evidenced in the past earthquake events such as the 1999 Kocaeli earthquake in Turkey, the 2008 Wenchuan earthquake in China, the 2009 L'Aquila in Italy, the March 11, 2011, Great East Japan earthquake, and the February 22, 2011, Christchurch earthquake in New Zealand. However, worldwide, building structures have been designed and built for a single traditional earthquake regulated in older or even in modern seismic codes. In scenarios of seismic sequences, the structures were damaged in the mainshocks, and the mainshock-damaged structures become increasingly vulnerable and easily collapse during the aftershocks, which were not taken into account in the design. Due to the seismology characteristics of strong earthquakes, the time gap between mainshocks and aftershocks is too short to conduct any repair, leading to high potential of collapse for the mainshock-damaged structures during the aftershocks. For example, USGS [2] reported that, in the 1999 Kocaeli earthquake in Turkey, the mainshock with magnitude 7.4 on 17 August was followed by the aftershock with magnitude 5.9 on 13 September. The aftershock resulted in the loss of seven lives and collapse of many buildings, which were only slightly damaged in the mainshock. Similar loss of lives and damage of buildings due to aftershocks have been reported by [3, 4]. Mitigating the risk of structures under seismic sequences is thus of great importance and urgent demand because, worldwide, building structures were designed based on seismic codes which employed single design for earthquakes.

Fibre reinforced polymer (FRP) has been widely proven to be a material of choice in seismic retrofitting because FRP has a high tensile strength, lightweight, and flexible

applications. Worldwide, a large portion of reinforced concrete (RC) structures are identified to be highly vulnerable to earthquakes. To address this issue, extensive research has been devoted to the FRP applications on improving the seismic performance for deficient RC structures. FRP can be used to improve the flexural strength [5, 6], torsional strength [7], and ductility of concrete by confinement [8–11]. The absorption energy [12–14], strength [13–15], and ductility [13, 15] of members confined by FRP considerably increased. Numerous studies indicated that FRP retrofitting of structures can significantly improve the seismic capacity and performance of structures as reviewed in the following. FRP confinement retrofitting increased 1.5-fold the seismic capacity of a tested four-storey RC frame as reported by Balsamo et al. [16]. A similar conclusion was found for the full-scale three-storey gravity-load designed RC frames [17, 18], in which columns were wrapped by FRP while beams were bonded by FRP to increase flexural capacity. In addition, the deformation capacity of FRP retrofitted structures increased [18], while the damage of such structures reduced [18, 19]. In an experimental study, Garcia et al. [20] confirmed that the seismic performance and desirable beam-sway mechanism of their tested frame were achieved by FRP wraps in combination with web-bonded sheets. Wang et al. [21] experimentally reported that, of the 3D four-storey FRP-retrofitted RC frames, the seismic capacity significantly increased, while the maximum inter-storey drifts decreased considerably. FRP retrofitting respectively increased 1.5-fold and 2.3-fold the shear force and energy dissipation capacity of RC frames as reported by Mortezaei et al. [22]. FRP wraps significantly increase the seismic performance and ductility of nonductile RC frames [23]. It is worth emphasizing that the previously mentioned studies were of single traditional earthquake ground motions or the effects of aftershocks were ignored.

Seismic risk assessment of structures subjected to earthquakes with aftershocks is an interesting and hot topic which has increasingly attracted researchers. Several researchers employed single-degree-of-freedom (SDOF) systems to investigate the effects of seismic sequences. Although SDOF systems take into account only the first structural period, they provide much better understanding on the effect of aftershocks on structures. For example, aftershocks affected the damage potential [24–26], inelastic displacement demand [27–29], ductility demand [26, 30, 31], behaviour factor [32, 33], and reduction factor of strength [32, 34]. Moving to multistorey frame structures subjected to seismic sequences, Faisal et al. [35] indicated that earthquakes with one and two aftershocks, respectively, increased 1.4-fold and 1.3-fold the storey ductility demand of 3–18 storey RC frames compared with single earthquakes. Aftershocks increased the fragility [36] and additional loss [37] of RC building structures. Hatzigeorgiou and Liolios [38] studied the nonlinear responses of RC frames designed based on older seismic codes subjected to seismic sequences and confirmed that the aftershocks increased the displacement demands and damage to structures. Ruiz-García et al. [39] employed artificial sequences to investigate the nonlinear responses of RC structures with different number of stories, and they indicated that the structural responses were significantly affected by the relationship between the mainshock-damaged structural period and the predominant period of aftershock. Hosseinpour and Abdelnaby [36] confirmed that the mainshock damage, number of storeys, and earthquake regions were important parameters that affected the fragility curves. Hatzivassiliou and Hatzigeorgiou [40] studied the effects of seismic sequences on the inelastic responses of 3D RC frames and indicated that the aftershocks increased the displacement while the directions of earthquake ground motions significantly affected the structural ductility demand. Most recently, Yang et al. [41] evaluated the damage demand of an eight-storey RC frame subjected to near-fault seismic sequences and the results showed that the aftershocks decreased the collapse capacity of structures while the near-fault pulse-type aftershocks increased the storey damage demand. Shin et al. [42] analysed the responses of three-storey frames with and without FRP retrofitting subjected to mainshock-aftershock sequences. They concluded that FRP reduced the drift demand, while the number of FRP plies had a marginal effect in the drift demand.

Studies published in the literature related to earthquakes and FRP retrofitting can be divided into two main groups: (1) the use of FRP to retrofit structures subjected to single earthquakes and (2) the effects of mainshock-aftershock sequences on original structures (without FRP retrofitting). However, to the best of the authors' knowledge, studies on using FRP to mitigate the seismic risk of RC structures subjected to near-fault mainshock-aftershock sequences are seldom found in the literature; this study is aiming at this direction. Particularly, the effectiveness of FRP retrofitting to reduce the seismic damage and collapse risk of building structures located in near-fault regions with and without aftershocks was investigated in this paper. To achieve this aim, a four-storey RC frame representing low-rise building structures was selected. The frame was retrofitted using FRP wraps at plastic hinges. The original and FRP retrofitted frames were subjected to near-fault earthquakes and mainshock-aftershock sequences. Inelastic time history analyses (ITHA) of these frames were carried out. The results of ITHA were used for damage analyses using a cumulative damage model. The conclusions were made based on the comparisons of four cases: (1) original structure subjected to single mainshocks, (2) original structure subjected to mainshock-aftershock sequences, (3) FRP retrofitted structure subjected to single mainshocks, and (4) FRP retrofitted structure subjected to mainshock-aftershock sequences. It is worth mentioning that the mainshocks used in this study are of near-fault earthquakes.

2. Near-Fault Earthquakes and Selection

Near-fault earthquake ground motions of the 1966 Parkfield and 1971 San Fernando were a milestone [43] of recognition on their greatly different characteristics to those of far-fault ground motions [44, 45]. This milestone has surged huge studies on the effects of near-fault earthquakes on structures [45]. Bertero et al. [46] were the pioneers in pointing out the

special characteristics of near-fault ground motions. Near-fault ground motions generally have high peak ground acceleration (PGA) [47], high velocity [33, 47, 48], and large displacements [49, 50]. More importantly, near-fault ground motions are characterized by pulse-like [51] and long pulse-like period (2–5 s) [48, 52, 53].

Due to the above critical characteristics, near-fault earthquakes have been identified as damaging events to structures. The pulses of near-fault ground motions impose high demand and energy to structures [45, 54]. Choi et al. [55] experimentally studied the effects of near-fault earthquakes on RC bridge columns and concluded that moderate near-fault ground motions imposed large residual displacements. Tsai et al. [56] reported that a large portion of damaged buildings in the September 21, 1999, Chi-Chi earthquake was low-rise. Cao et al. [57] confirmed that low-rise deficient RC structures are extremely vulnerable to near-fault ground motions. Near-fault earthquakes imposed a higher displacement demand on RC frames [58, 59] than far-fault earthquakes. Mazza and Vulcano [60] investigated the responses of three-to-twelve-storey RC frames subjected to near-fault earthquakes and pointed out the shortcomings of seismic codes for designing structures in near-fault regions, especially with soft soil. Recently, Cao [61] analysed the damage of an RC bridge pier under 200 near-fault pulse-type motions and 200 far-fault motions. He found that near-fault earthquake imposed high collapse potential to the pier, and the damage of the pier was mainly caused by the pulses. In addition, the damage index increased sharply at the pulse, leading to very short durations to collapse (about 2.3–2.5 s). The effect of aftershocks on in-filled structures [62] or braced structures [63] was also investigated by researchers.

Figure 1 shows the design response spectrum (the red curve) which was established for structures located in near-fault regions of zone four ($Z = 0.4$) based on UBC code [64]. The regions with soil type D and seismic source type B were assumed. The closest distance to seismic source was 5 km. The near-source factors $N_a = 1.0$ and $N_v = 1.2$. The seismic coefficients were $C_a = 0.44N_a$ and $C_v = 0.64N_v$. The near-fault ground motions were selected using PEER [65] and scaled to match the design response spectrum. The match was in the range from 0.2 T to 1.5 T, in which $T = 0.76438$ s was the fundamental period of the frame (see Section 4). Records of near-fault earthquakes with magnitudes close to 7.5 were selected to use as mainshocks. These selected near-fault motions were scaled to match the design response spectrum. Table 1 shows the selected near-fault ground motions in which RSN is the record series number. The scale factors are also included in the third column of this table.

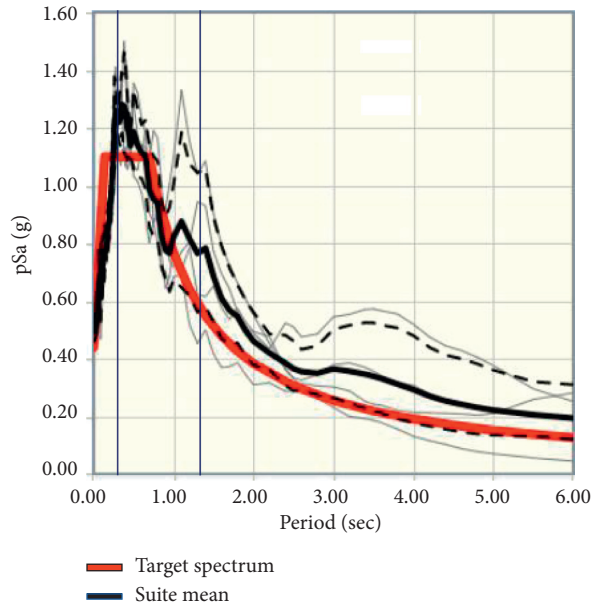

Figure 1: Design response spectrum for structures located in near-fault regions.

3. Mainshock-Aftershock Sequences

Three approaches have been implemented by researchers to obtain mainshock-aftershock sequences: (1) repeating the selected records [29, 32, 33, 66, 67], (2) randomizing [24, 29, 38, 66–68], and (3) using real seismic sequences [66]. The repeating method is simple but less appropriate due to the different characteristics, for example, duration and frequency content between mainshocks and aftershocks [27, 67, 69]. On the contrary, using real seismic sequences seems to be the most appropriate as confirmed by researchers [69]. However, the number of real mainshock-aftershock records is quite limited in the literature database to use for structural probabilistic analytical scenarios [70]. In addition, the intensity of these real mainshocks and aftershocks is quite diverse, leading to difficulty in obtaining general conclusions. Therefore, the second approach is widely used by researchers [24, 29, 38, 66–68] because it can represent the stochastic relationships between mainshocks and aftershocks; this approach is thus adopted in this paper.

Aftershocks are triggered by mainshocks due to stress changes during the mainshocks [71]; there is therefore a relationship between the magnitudes of mainshocks and aftershocks. This relationship can be expressed by Bath's law [72], which is one of the widely used scaling laws for concerning aftershocks. This law states that the difference between a mainshock and its largest aftershock is 1.2, regardless the magnitudes of the mainshocks. Bath's law was later modified by Shcherbakov [73] to describe the magnitude–frequency distribution of aftershocks based on Gutenberg-Richter [74] and Bath [72] laws. The modified form is expressed by (1), where N_{as} is the number of aftershocks whose magnitudes are larger than or equal to a value M_{as}; M_{as} is the magnitude of inferred largest aftershock; M_{ms} is the magnitude of mainshocks; b is a constant taken as 1 [75]; ΔM is the difference between M_{ms} and the inferred largest aftershock magnitude:

$$\log_{10}\left[N_{\text{as}}\left(\geq M_{\text{as}}\right)\right] = b\left(M_{\text{ms}} - \Delta M - M_{\text{as}}\right). \quad (1)$$

Seismic sequences with single aftershocks, which were commonly used in previous studies [24, 67], are adopted in this paper. When the number of aftershock is 1, the left side

of the (1) is 0; thus, the relationship between the magnitudes of mainshocks and aftershocks is described by

$$M_{\mathrm{ms}} - M_{\mathrm{as}} = \Delta M. \quad (2)$$

Different values of ΔM have been proposed by researchers. Based on worldwide earthquake sequences, Felzer et al. [76] proposed $\Delta M = 1.0 - 1.4$, while Tahir et al. [77] proposed the value 1.2 which is the average value of the range 1.0–1.4. Based on 10 earthquake sequences in California, Shcherbakov [73] proposed $\Delta M = 1.16$ which is also close to the above average values. In another study, using seismic sequences in Taiwan, Chen and Wang [78] proposed a lower value of 0.83. Except the value 0.83 for seismic sequences in Taiwan, the value 1.2, which was originally proposed by Båth [72] and used by Zhai et al. [24], is adopted in this study. Thus, records with magnitudes close to 6.3 were selected for aftershocks using PEER ground motion database [65]. It is worth mentioning that no pulse-like motions were selected for aftershocks because of the gentler manner of aftershocks caused by stress changes from mainshocks. The information of the selected records is shown in Table 2, including the directions and predominant periods of the seismic records.

The combinations of the eight mainshocks of Table 1 and eight aftershocks of Table 2 were described as follows. One record of mainshocks was connected with one record of aftershocks to form a sequence. Each record appeared only one time in the sequence combinations. The random combinations also reflected the unpredictability on the characteristics of a seismic sequence. The following conditions were used for combining mainshock-aftershock sequences:

(1) The modified Bath's law: the relationship between the magnitudes of mainshocks and aftershocks is shown in (2)

(2) The characteristic of aftershocks pointed out by Ruiz-García [69]: the predominant period of an aftershock is shorter than its mainshock

(3) The magnitude of the mainshocks was unchanged, while the magnitude of aftershock was scaled to satisfy the condition $\mathrm{PGA}_{\mathrm{ms}}$: $\mathrm{PGA}_{\mathrm{as}}$ = 1.0000: 0.8526 recommended by Hatzigeorgiou and Beskos [29]; this agrees with the characteristic pointed out by Ruiz-García [69] that the amplitude of an aftershock is smaller than that of mainshock

Table 3 shows the results of sequence combinations. The penultimate column shows the difference between the magnitudes of mainshocks and aftershocks, which varies from 1.2 to 1.42. The last column of Table 3 shows the predominant periods of mainshocks and aftershocks. As can be seen, the predominant periods of mainshocks are longer than those of the corresponding aftershocks. The time gap between the mainshock and aftershock of a seismic sequence has been differently selected by researchers; however, it seems to be based on the same criterion that the time is long enough for damping to cease the movement of structures after the mainshock. In this study, the time gap between the mainshock and aftershocks is selected to be 10 s.

4. Four-Storey RC Frames and Inelastic Time History Analyses

Figure 2 shows a nonductile four-storey frame with details of reinforcement and cross-sections of beams and columns [79] which is revisited in this paper. The design gravity load included dead load (DL) 30 kN/m, live load (LL) 10 kN/m on beams, and self-weight of the structure. The building was assumed to be located in the seismic zone with soil type D in accordance with FEMA 356 [80]. The design ground acceleration was $0.3g$. UBC code [64] was used to compute the lateral seismic load. The lowest ratio of the total bending moment capacity of columns $\sum M_c$ to that of beams $\sum M_b$ was 1.226 and thus satisfies the condition $\sum M_c \geq 1.2 \sum M_b$ regulated in ACI [81]. The compressive concrete strength was 25 MPa and yield steel stress was 420 MPa. Diameter of stirrups was 10 mm.

Due to the large spacing of transverse reinforcement, the structure is nonductile and becomes vulnerable to earthquakes. In addition, near-fault earthquakes and aftershocks were not included in the design. Thus, retrofitting is required to mitigate the seismic risk for such structures. Retrofitting using FRP wraps is identified an appropriate approach because it well provides the external confinement conditions to supplement the deficiency of internal confinement. Amongst many types of FRP, GFRP has been the most technically and economically suitable FRP type for confinement of RC structures [19, 23, 79]. The tensile strength, elastic modulus, and thickness of unidirectional GFRP sheets, respectively, are 3241 MPa, 72397 MPa, and 0.589 mm [82]. The aim of this paper is to evaluate the damage potential reduction of FRP retrofitting on RC frames subjected to seismic sequences; thus, two GFRP layers were applied to columns. The length of GFRP wrapped columns is assumed to be twice the plastic hinge length l_p. To avoid early failure of FRP and improve the effectiveness of the GFRP confinement [83], rounding 50 mm radius at corners of all columns was applied. It is highlighted that GFRP wraps result in enhancement of compressive strength and ductility of concrete; thus, it has a negligible effect on the plastic hinge length as indicated by Sheikh and Yau [13]. The locations of plastic hinges therefore unchanged.

The lump technique employed for modelling RC structures under earthquake excitations [19] is used in this study. The details of the modelling can be found in [19], while only brief information of the modelling is described herein for convenience to readers. The moment-curvature analyses were firstly conducted for plastic sections using fibre model conducted in Matlab. The simple stress-strain model of steel and the model of confined concrete proposed by Park et al. [84] were employed in the analyses. Moment is obtained by increasing the curvature up to its ultimate. The ultimate corresponds to the ultimate strain of concrete $\varepsilon_{\mathrm{cm}} = 0.004 + 1.4\rho_s f_{yh}\varepsilon_{suh}/f'_{cc}$ [85] or longitudinal steel $\varepsilon_{\mathrm{sm}} = 0.6\varepsilon_{\mathrm{su}}$ [85], whichever occurs first. These analyses were conducted for all plastic hinge

Table 1: Selected near-fault mainshock records.

No.	RSN	Scale factor (g)	Event	Year	Station	Magnitude	Predominant period (sec)	Direction
1	1176	1.868	Kocaeli, Turkey	1999	Yarimca	7.51	0.520	H-1
2	1176	1.868	Kocaeli, Turkey	1999	Yarimca	7.51	0.420	H-2
3	1493	2.610	Chi Chi, Taiwan	1999	TCU053	7.62	0.360	H-1
4	1493	2.610	Chi Chi, Taiwan	1999	TCU053	7.62	0.680	H-2
5	1515	2.238	Chi Chi, Taiwan	1999	TCU082	7.62	0.380	H-1
6	1515	2.238	Chi Chi, Taiwan	1999	TCU082	7.62	0.640	H-2
7	4458	2.014	Montenegro, Yugoslavia	1981	Hotel Olympic, Ulcinj	7.10	0.260	H-1
8	4458	2.014	Montenegro, Yugoslavia	1981	Hotel Olympic, Ulcinj	7.10	0.340	H-2

Table 2: Selected records for aftershocks.

No.	RSN	Event	Year	Station	Magnitude	Predominant period (sec)	Direction
1	3468	Chi-Chi, Taiwan-06	1999	TCU067	6.30	0.360	H-1
2	3268	Chi-Chi, Taiwan-06	1999	CHY028	6.30	0.400	H-2
3	3467	Chi-Chi, Taiwan-06	1999	TCU065	6.30	0.340	H-2
4	2605	Chi-Chi, Taiwan-03	1999	TCU049	6.20	0.660	H-1
5	2709	Chi-Chi, Taiwan-04	1999	CHY035	6.20	0.360	H-1
6	3274	Chi-Chi, Taiwan-06	1999	CHY142	6.30	0.620	H-2
7	3560	Taiwan SMART1 (5)	1979	SMART1 I09	5.90	0.240	H-2
8	3570	Taiwan SMART1 (5)	1979	SMART1 M12	5.90	0.300	H-2

Table 3: Combinations of seismic sequences.

Sequence	RSN	Scale factor (g)	Event	Year	Station	Magnitude	ΔM	Predominant period (sec)
1	1176	1.868	Kocaeli, Turkey	1999	Yarimca	7.51	1.21	0.520
	3468	$0.8526PGA_{ms}$	Chi-Chi, Taiwan-06	1999	TCU067	6.30		0.360
2	1176	1.868	Kocaeli, Turkey	1999	Yarimca	7.51	1.21	0.420
	3268	$0.8526PGA_{ms}$	Chi-Chi, Taiwan-06	1999	CHY028	6.30		0.400
3	1493	2.610	Chi Chi, Taiwan	1999	TCU053	7.62	1.32	0.360
	3467	$0.8526PGA_{ms}$	Chi-Chi, Taiwan-06	1999	TCU065	6.30		0.340
4	1493	2.610	Chi Chi, Taiwan	1999	TCU053	7.62	1.42	0.680
	2605	$0.8526PGA_{ms}$	Chi-Chi, Taiwan-03	1999	TCU049	6.20		0.660
5	1515	2.238	Chi Chi, Taiwan	1999	TCU082	7.62	1.42	0.380
	2709	$0.8526PGA_{ms}$	Chi-Chi, Taiwan-04	1999	CHY035	6.20		0.360
6	1515	2.238	Chi Chi, Taiwan	1999	TCU082	7.62	1.32	0.640
	3274	$0.8526PGA_{ms}$	Chi-Chi, Taiwan-06	1999	CHY142	6.30		0.620
7	4458	2.014	Montenegro, Yugoslavia	1979	Hotel Olympic, Ulcinj	7.10	1.20	0.260
	3560	$0.8526PGA_{ms}$	Taiwan SMART1 (5)	1981	SMART1 I09	5.90		0.240
8	4458	2.014	Montenegro, Yugoslavia	1979	Hotel Olympic, Ulcinj	7.10	1.20	0.340
	3570	$0.8526PGA_{ms}$	Taiwan SMART1 (5)	1981	SMART1 M12	5.90		0.300

sections of the frame. Then, these moment-curvature curves were converted to moment-rotation curves by multiplying with the plastic hinge length. Simple plastic hinge length $l_p = h$ proposed by Sheikh and Khoury [86] was adopted in this paper. These moment-rotation curves were used for the properties of the plastic hinges in SAP2000 [87]. Figure 3(a) shows the four-storey frame model using 56 nonlinear Link elements. The locations of these elements are at the middles of the plastic hinges. These Link elements behave nonlinearly and hysterically and include the degradations of strength and stiffness of plastic hinges under earthquake loading. The Takeda hysteretic model [88] appropriately includes not only those characteristics but also the concrete crack which is considered as the onset of damage. This Takeda [88] model is thus used in this paper. The Takeda [88] model is shown in Figure 3(b), while its details can be found in [88].

The mechanical properties of concrete confined by FRP significantly improved [8, 9, 89–92]. There are two trends for developing stress-strain models for FRP confined concrete: with and without including the confinement effect of internal transverse reinforcement. Stress-strain models with the inclusion of internal transverse reinforcement exhibit the complexity due to the different confinement applied to the concrete core and the concrete cover. The concrete core is confined by both FRP and transverse reinforcement, while the concrete cover is confined only by FRP. In addition, the interaction between the internal confinement of transverse reinforcement and the external confinement of FRP is complicated. Importantly, FRP wrap

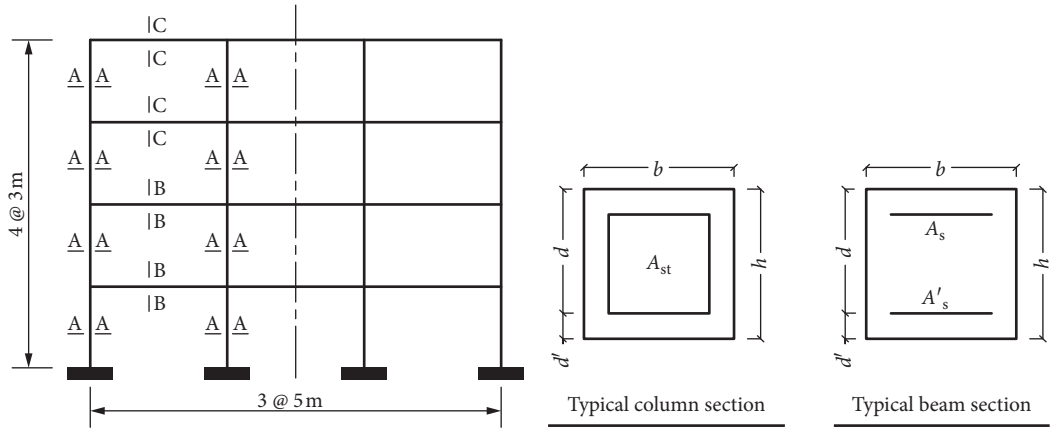

Section	b mm	h mm	d mm	d' mm	A_{st} mm^2	A_s mm^2	A'_s mm^2	Spacing of stirrups mm
A-A	500	500	440	60	16ϕ18	—	—	455
B-B	500	500	440	60	—	6ϕ22	4ϕ22	175
C-C	500	500	440	60	—	6ϕ18	3ϕ18	250

Figure 2: Four-storey frame.

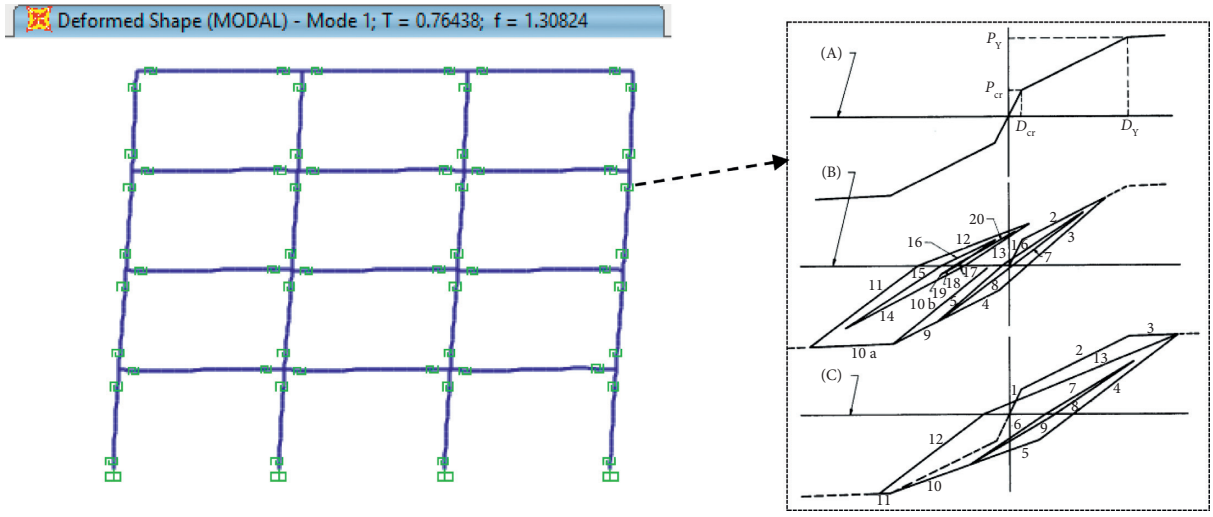

Figure 3: Modelling for inelastic analyses. (a) Modelling. (b) Hysteretic behaviour [88].

retrofitting is often applied for structures with poor internal confinement. Thus, this poor internal confinement of transverse reinforcement is ignored in this study. Lam and Teng [8, 89] model of FRP confined concrete ignored the effect of internal transverse reinforcement, which has been used by researchers [23, 93]. In addition, this model is the most suitable for circular and rectangular columns [93] and is thus used in this paper. The rupture strain of GFRP is taken as $\varepsilon_{h,\text{rup}} = k_\varepsilon \varepsilon_{\text{frp}}$, in which ε_{frp} is the ultimate tensile strain of GFRP; k_ε is the FRP strain efficiency factor. The value $k_\varepsilon = 0.624$ proposed by [8], which is close to the value 0.62 statistically found by Baji [94], is adopted in this paper.

5. Verification of the Inelastic Time History Analyses

The modelling technique expressed in Section 4 was verified using the test results of [20, 95]. A brief description of the tested two-storey RC frame is described here for convenience to readers, while its details can be found in [20, 95]. Figure 4(a) displays the general view of the tested two-storey RC frame and Figure 4(b) shows the cross-sections and reinforcement details of columns and beams. The gravity load was the self-weight of the frame and 45 kN steel plates

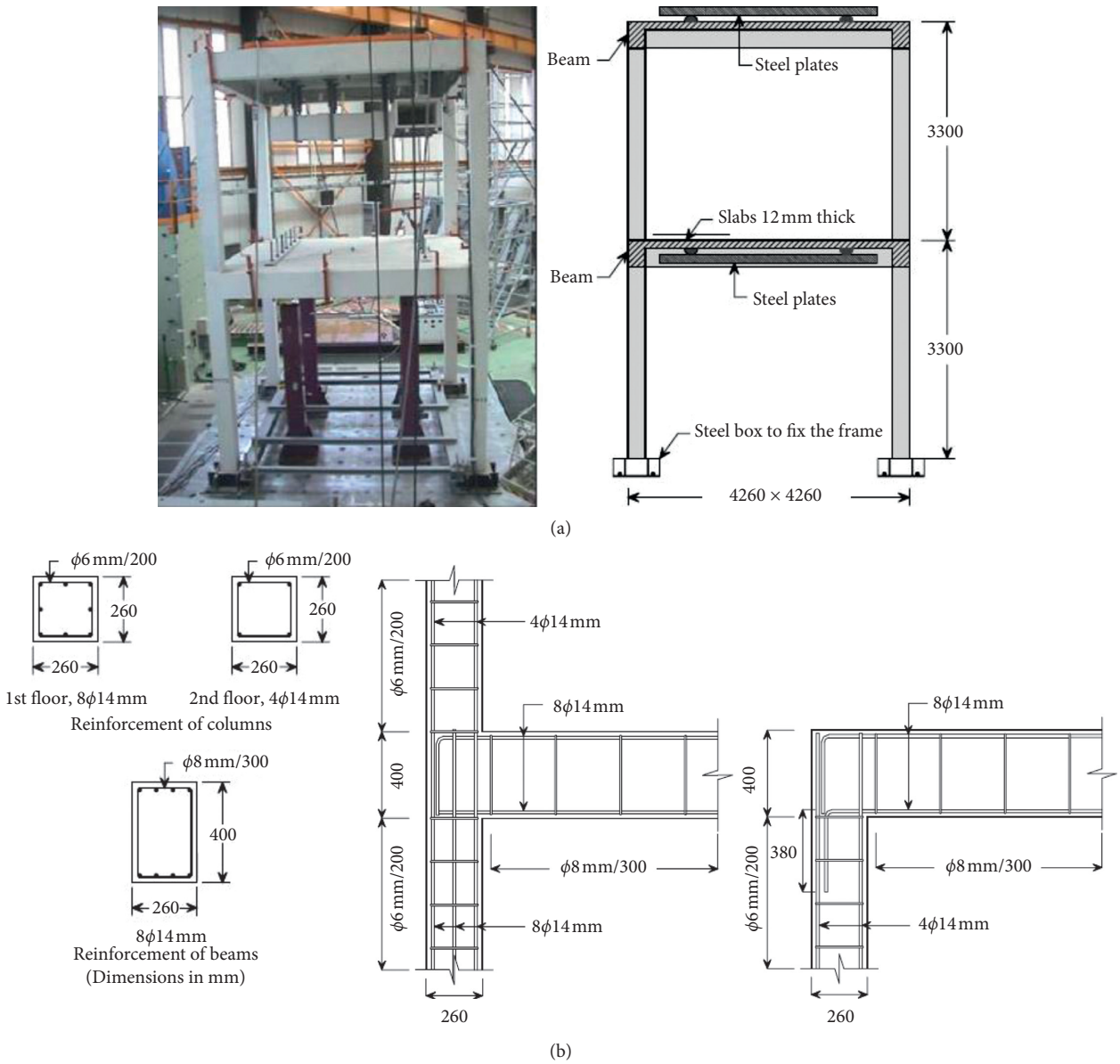

Figure 4: The tested two-storey RC frame [20, 95]. (a) General view. (b) Cross-sections and reinforcement details of columns and beams.

attached to floors as can be seen in Figure 4(a). The unit weight of concrete was 24 kN/m^3. The compressive strength, tensile strength, and elastic modulus of concrete were 20 MPa, 2 MPa, and 25545 MPa, respectively. The yield strength, ultimate strength, and elastic modulus of steel were 551 MPa, 656 MPa, and 200 GPa, respectively. The transverse steel of columns was ϕ6 mm and that of beams was ϕ8 mm.

The modelling technique expressed in Section 4 was used to model tested two-storey RC frame in SAP2000 [87]. The first and second analytical periods yielded from the SAP2000 frame model are compared with those obtained from experiments [20, 95], and a good agreement was achieved as shown in Table 4.

The SAP2000 [87] frame model was then subjected to the ground excitation PGA of 0.05 g, which was used in the experiments [20, 95]. Time history nonlinear analysis was carried out, and time history displacements were obtained. These obtained time history displacements of the first and second storeys were compared with those obtained from the experiment with good agreement as shown in Figures 5 and 6, respectively.

6. Response/Damage Results and Discussion

Inelastic time history analyses of the original and FRP-retrofitted frames were performed. The hysteretic behaviours of all nonlinear Link elements under every seismic sequence were captured to be later used for damage analyses. Figure 7 shows examples of hysteretic behaviors of the plastic hinge at the bottom ends of inner columns. The effect of near-fault earthquakes can be observed in this figure. When the pulses of near-fault ground motions arrive, the frames responded by one or a few large plastic cycles. These large plastic cycles had high deformations; consequently, a high amount of hysteretic energy was absorbed by the structures.

Table 4: The first and second analytical periods (s) obtained from analysis and experiment.

Period	Analysis	Experiment [20, 95]
First mode	0.54	0.53
Second mode	0.18	0.18

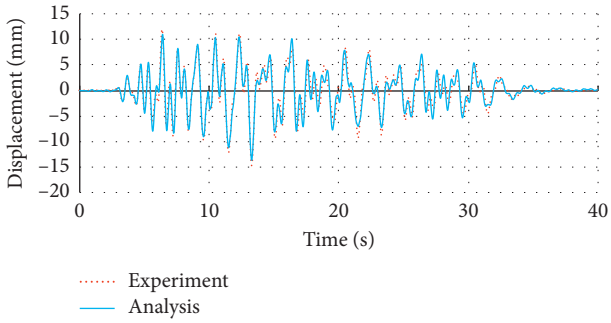

Figure 5: History lateral displacements of the first storey obtained from analysis and experiment [20, 95].

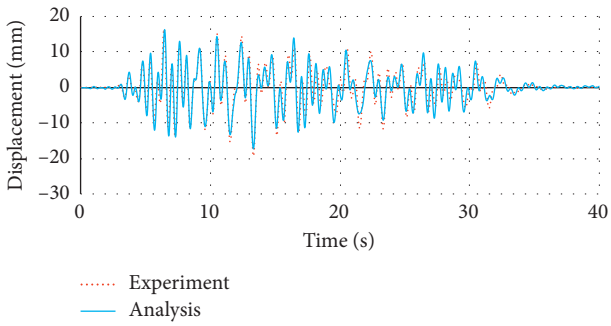

Figure 6: History lateral displacements of the second storey obtained from analysis and experiment [20, 95].

The hysteretic moment-rotation behaviors of all plastic hinges in the frames were exported to Excel files which were then imported to Matlab to compute the damage indices using a damage model. Cumulative damage models are more appropriate than the noncumulative damage models in assessment of structures subjected to earthquakes. The damage index should have the magnitude varying between 0 and 1 inclusively. The damage index should be 0 when the structures work in their elastic range or no damage, and the damage index should be 1 when the structures totally collapse. In addition, the damage index should increase with the increase of force, displacement, or number of loading cycles. The damage model proposed by Cao et al. [96] shown in (3), followed by (4) and (5), satisfies the just-mentioned characteristics and is thus selected to use in this paper. In this model, $E_{h,1\text{collapse}}$ and $E_{h,1y}$ are, respectively, the hysteretic energy of one complete ultimate and yielding cycle; N is the equivalent number of yielding cycles to collapse; i is the equivalent number of yielding cycles at the current time of loading ($i \le N$); $\alpha = 0.06$ is a modification factor. Table 5 shows the description and classification of damage levels based on the ID magnitude. The legends for the damage levels are also included in Table 5, and these legends are used to plot the damage states of frames in Section 6:

$$\text{DI} = \left[\frac{E_h}{E_h + E_{\text{rec}}}\right]^{\alpha(N-i)}, \tag{3}$$

$$N = \frac{E_{h,1\text{collapse}}}{E_{h,1y}}, \tag{4}$$

$$i = \frac{E_h}{E_{h,1y}}. \tag{5}$$

Figure 8 shows the variations of damage indices of the original and retrofitted frames subjected to seismic sequences. On the left in Figure 8 are the variations of DI of the original frame, while on the right column are those of the FRP retrofitted frames. Three aspects can be obtained from Figure 8. Firstly, the effects of near-fault pulses on the original FRP retrofitted frames are significant as can be seen in Figure 8. At the arrival of near-fault pulses, the response structures are characterized by one or few large plastic cycles, forcing the structures to absorb a large amount of energy; consequently, the damage indices sharply increased. Secondly, Figure 8 shows the effects of aftershocks on the final damage indices of the frames under seismic sequences. The damage indices significantly increase when the aftershocks arrived. The increase of damage indices at the latter time of seismic sequences played an important role on the final damage state of the frame. Thirdly, Figure 8 shows that the FRP retrofitting exhibited its effectiveness in both mainshocks and sequences. The damage index caused by the mainshock for the FRP retrofitted frame is small and the frame has light damage. Because the strong mainshock caused only light damage to the FRP-retrofitted frame, the aftershock, which is normally weaker than the mainshock, can increase very limited amount of damage indices for the frame. This light damaged FRP-retrofitted frame thus has the low possibility to increase the damage index when the aftershocks occurred.

The average damage states of four cases of earthquakes are shown in Figure 9 for comparison. Figure 9 shows the damage states of the frames with and without FRP retrofitting under mainshocks with and without aftershocks. It is worth mentioning that the legends presented in Table 5 are used to read the damage levels in the frames. Figure 9(a) shows the severe damage state of the original frame subjected to mainshocks. This mainshock-damaged frame then collapsed when the aftershock occurs as shown in Figure 9(b). Thus, the effect of aftershock increases the damage one level from severe damage to collapse. The collapse initiated from the two middle columns of the first storey.

With the FRP retrofitting, the damage of the frame is significantly improved. Figure 9(c) shows the damage state of the FRP retrofitted frame subjected to mainshocks. The damage indices reduce from collapse to light damage, showing the effectiveness of the FRP retrofitting under mainshocks. The light damage occurred only at the

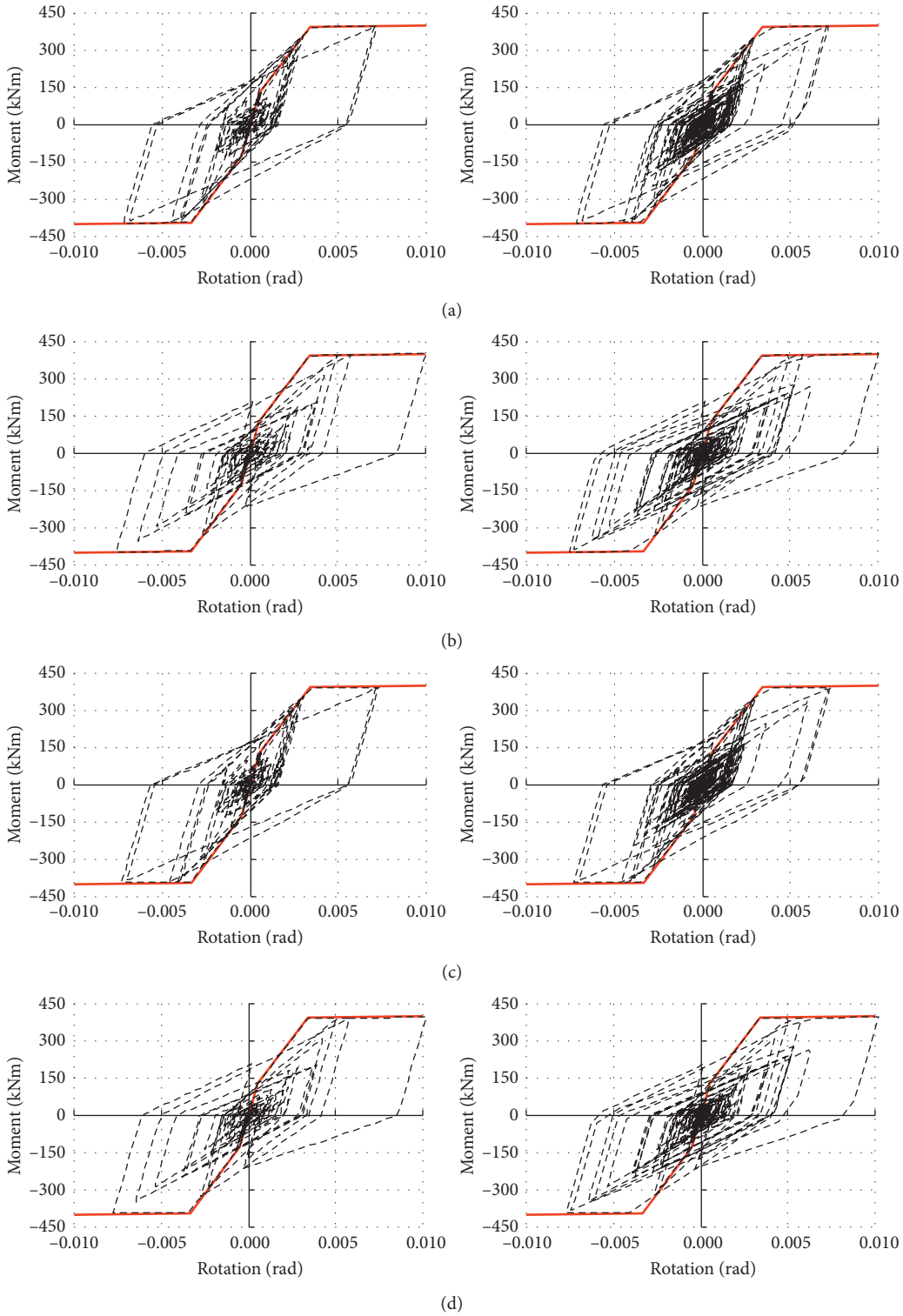

Figure 7: Examples of hysteretic behaviours of a plastic hinge under seismic sequences. (a) Original plastic hinge under mainshock (left) and seismic sequence 1 (right). (b) Original plastic hinge under mainshock (left) and seismic sequence 2 (right). (c) FRP retrofitted plastic hinge under mainshock (left) and seismic sequence 1 (right). (d) FRP retrofitted plastic hinge under mainshock (left) and seismic sequence 2 (right).

bottom ends of the first storey columns, while other plastic hinges experienced minor damage. The effect of aftershocks on FRP retrofitted frame is significant as can be seen in Figure 9(d). With light damage in the mainshocks shown in Figure 9(c), the damage indices of FRP retrofitted frame increase the damage one level from light damage (Figure 9(c)) to moderate damage (Figure 9(d)).

Table 5: Cao et al. [96] damage levels and the legends.

Legend	DI	Description
.	0–0.05	No or minor
+	0.05–0.25	Light
×	0.25–0.50	Moderate
▲	0.50–0.75	Severe
●	0.75–1.00	Collapse

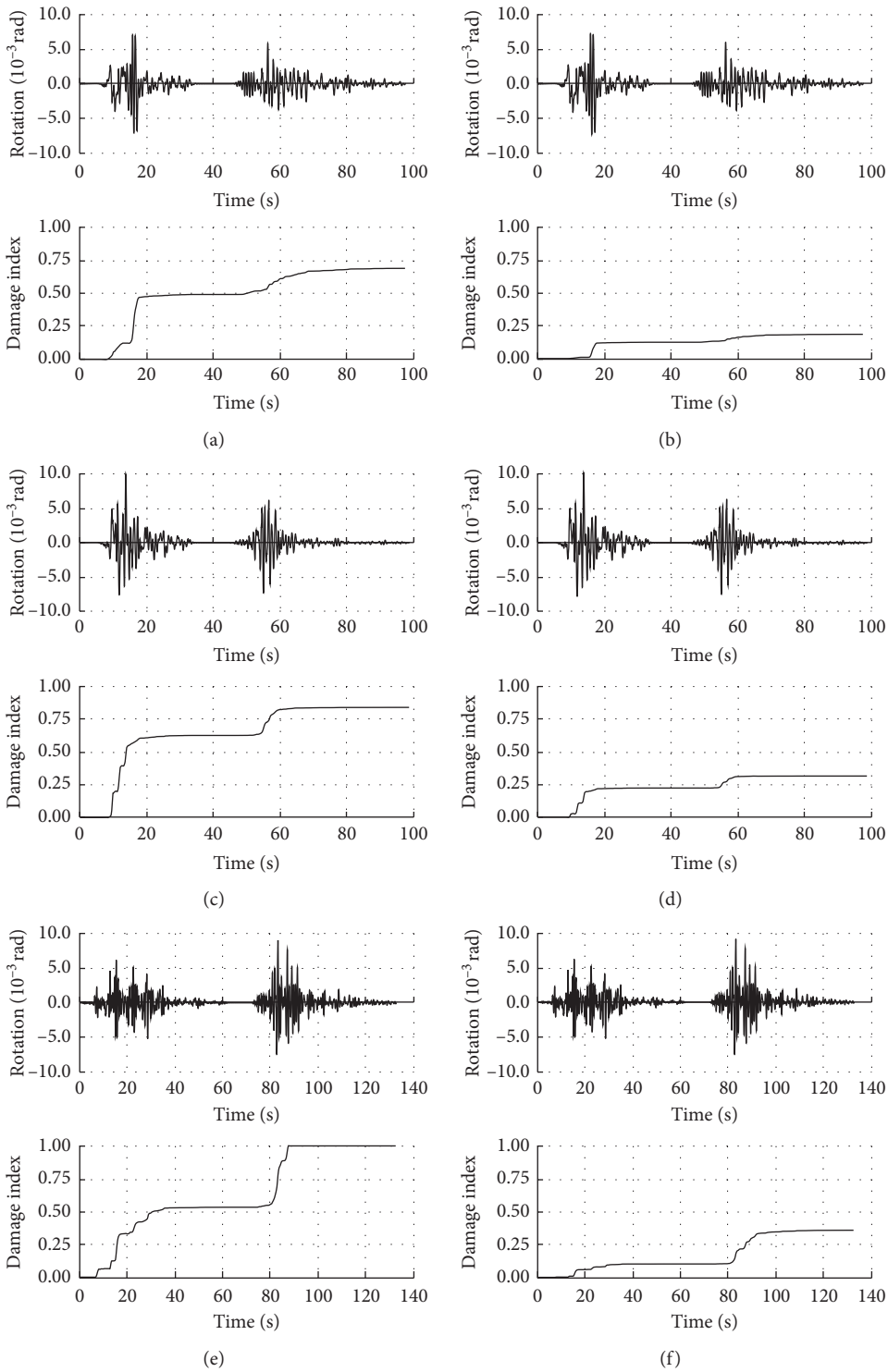

Figure 8: Continued.

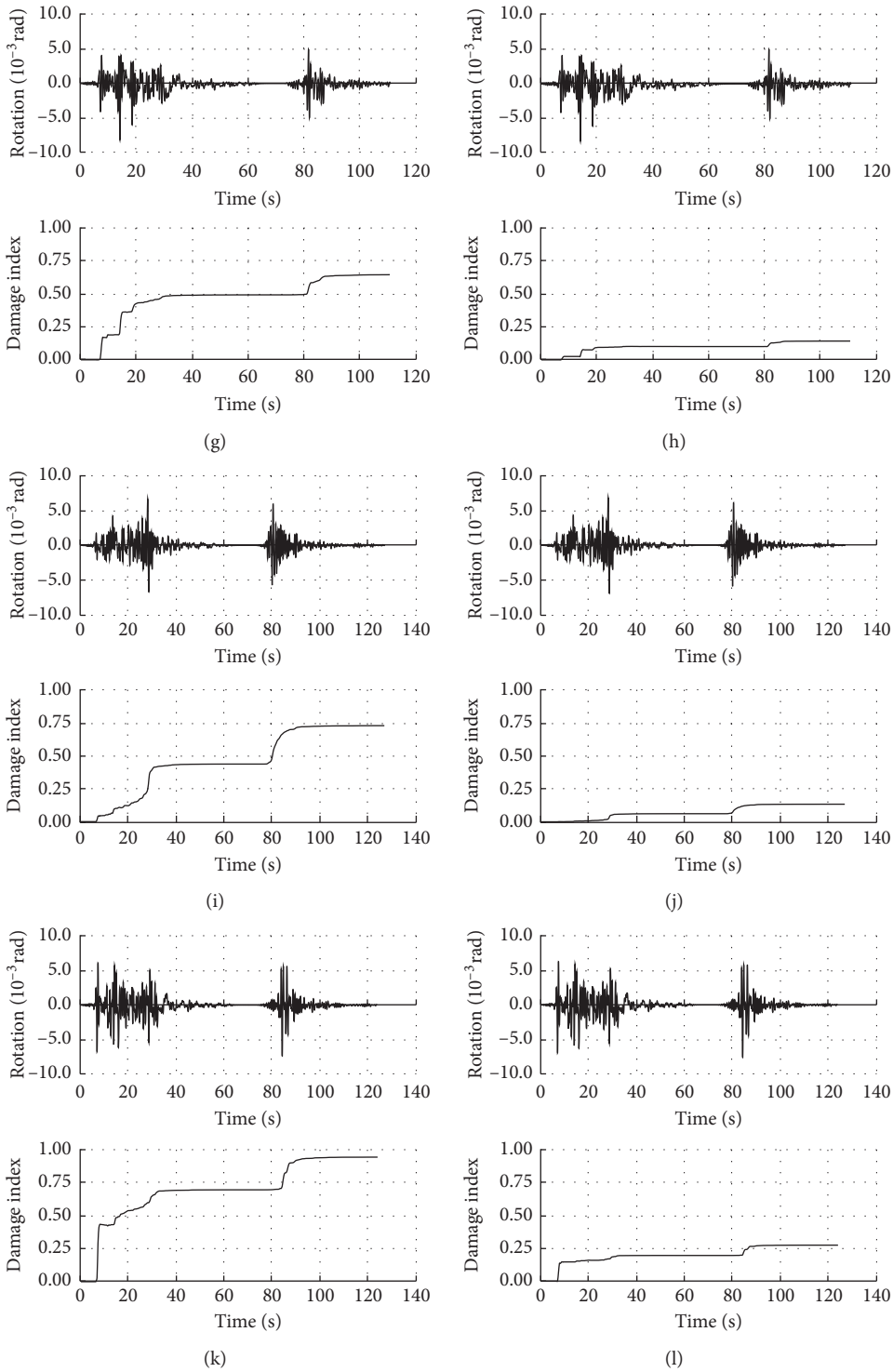

Figure 8: Continued.

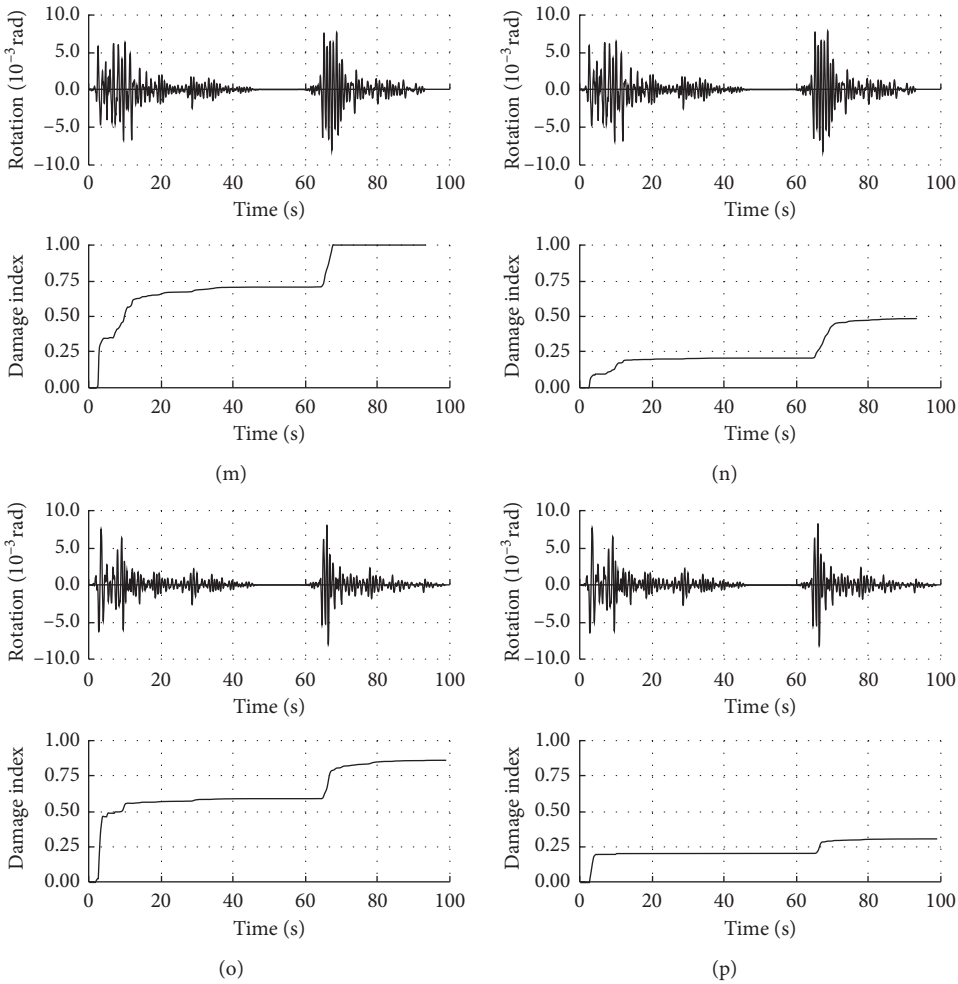

Figure 8: Variations of damage indices during seismic sequences. (a) Original frame under sequence 1. (b) FRP-retrofitted frame under sequence 1. (c) Original frame under sequence 2. (d) FRP-retrofitted frame under sequence 2. (e) Original frame under sequence 3. (f) FRP-retrofitted frame under sequence 3. (g) Original frame under sequence 4. (h) FRP-retrofitted frame under sequence 4. (i) Original frame under sequence 5. (j) FRP-retrofitted frame under sequence 5. (k) Original frame under sequence 6. (l) FRP-retrofitted frame under sequence 6. (m) Original frame under sequence 7. (n) FRP-retrofitted frame under sequence 7. (o) Original frame under sequence 8. (p) FRP-retrofitted frame under sequence 8.

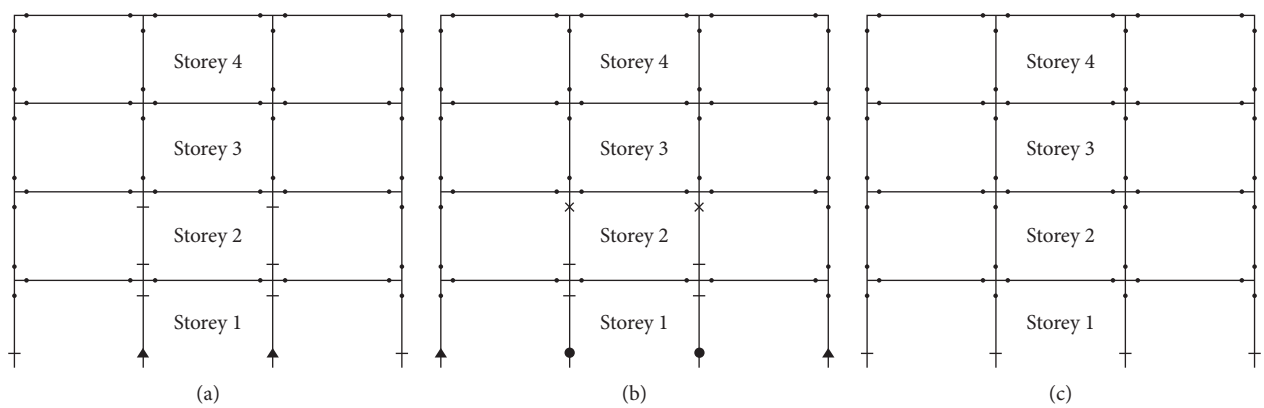

Figure 9: Continued.

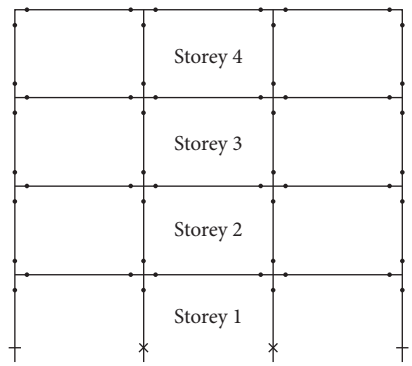

(d)

Figure 9: Damage states of the original and FRP-retrofitted frames. (a) Damage of original frame subjected to mainshocks. (b) Damage of original frame subjected to mainshock-aftershock sequences. (c) Damage of GFRP-retrofitted frame subjected to mainshocks. (d) Damage of GFRP-retrofitted frame subjected to mainshock-aftershock sequences.

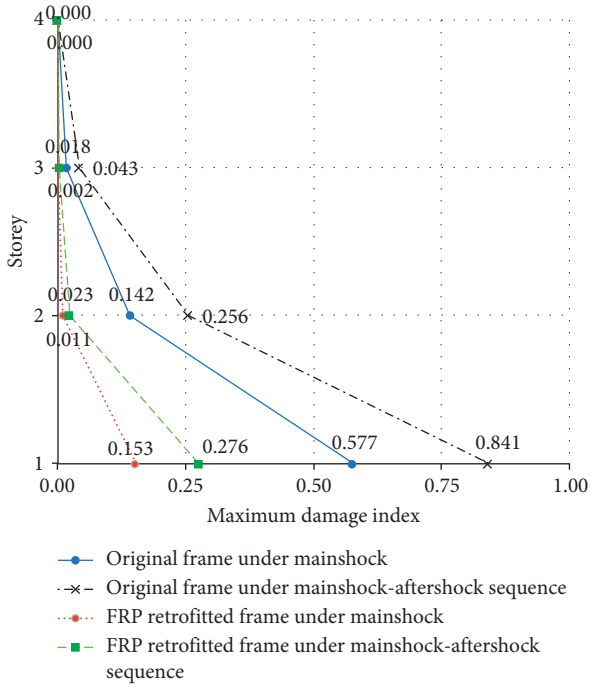

Figure 10: Maximum damage indices of storeys.

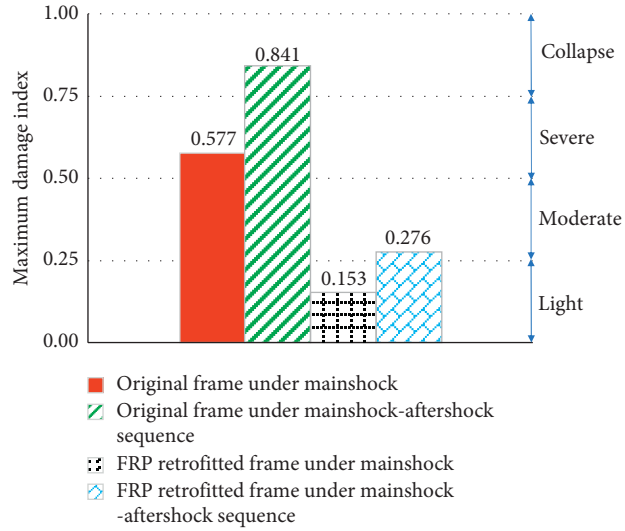

Figure 11: Maximum damage indices of the frames.

Figure 10 shows the distribution of storey damage indices, while Figure 11 shows the maximum damage indices of the original and FRP-retrofitted frames with and without aftershocks. The top storey experienced the least damage, while the most severe damage occurred in the bottom ends of the first storey. The first storey suffered the most severe damage. Of the original frame, the aftershock increased the damage index from 0.577 to 0.841, shifting the damage state from severe damage to collapse. On the contrary, the damage index of the FRP retrofitted frame was only 0.153 (light damage) in the mainshock and the damage index increased to 0.276 which is moderate damage.

Figures 10 and 11 also show an important aftershock effect. The aftershock increases the damage of the original frame one level from severe damage to collapse. Aftershocks have a similar effect on the FRP-retrofitted frame, increasing the damage one level from light damage to moderate damage. Thus, the collapse potential of aftershocks is high because the damage was cumulated during the mainshocks.

7. Conclusions

In this paper, a four-storey RC frame representing low-rise building structures was selected. The frame was designed with large spacing of stirrups, leading to low ductility. Also, the effects of near-fault earthquakes and aftershocks were not taken into account in the design. The frame was retrofitted using FRP wraps at the plastic hinge locations. Mainshock records were selected and scaled to match the design response spectrum

established for structures located in near-fault regions. Aftershock records were also selected based on the modified Bath's law, predominant periods, and PGAs of the mainshocks and aftershocks. Inelastic time history analyses of the original and FRP-retrofitted frames subjected to only near-fault mainshocks (traditional earthquakes) and near-fault mainshock-aftershock sequences were conducted. The hysteretic behaviours of plastic hinges resulting from inelastic time history analyses were then exported to compute the cumulative damage indices. The obtained results lead to the following conclusions.

(1) The effects of near-fault earthquakes to RC frames with or without FRP retrofitting are significant. The responses and damage indices of RC frames can be characterized by those at the arrival of the near-fault pulses. The damage indices of the frames subjected to near-fault mainshocks increase sharply in a very short time when the pulses of near-fault earthquakes arrived.

(2) Although the aftershocks are generally weaker than the mainshocks, the aftershocks significantly increase the damage indices of the frames, shifting the damage state of the frame from severe damage to collapse for the original frame and from light damage to moderate damage for the FRP retrofitted frame. This is attributed to the damage in the near-fault mainshocks which already weakens the frames; thus, the aftershocks easily increase a significant amount of damage indices. Importantly, the damage caused by aftershocks is critical in deciding the final damage states of the frames. Therefore, the traditional design using single earthquakes has shown its shortcomings, and it is strongly recommended to take the effects of aftershocks into account in the seismic design of RC structures.

(3) The damage indices of the FRP retrofitted frame were significantly lower than those of the original frame. The FRP wraps successfully reduced the damage of the frame two levels from severe damage (original frame) to light damage (FRP-retrofitted frame) when subjected to mainshocks and two levels from collapse to moderate damage when subjected to seismic sequences, showing the effectiveness of FRP retrofitting. FRP can thus be a material for strengthening RC structures located in near-fault regions which have strong mainshocks with or without aftershocks.

Data Availability

The data used to support the findings of this study are available from the corresponding author upon request.

Conflicts of Interest

The authors declare that they have no conflicts of interest.

Acknowledgments

This research was funded by Vietnam National University HoChiMinh City (VNU-HCM) under grant no. C2018-20-28.

References

[1] Y. Zhang, J. Chen, and C. Sun, "Damage-based strength reduction factor for nonlinear structures subjected to sequence-type ground motions," *Soil Dynamics and Earthquake Engineering*, vol. 92, pp. 298–311, 2017.

[2] USGS, "Implications for earthquake risk reduction in the United States from the Kocaeli, Turkey, earthquake of August 17, 1999," *Circular*, U.S. Geological Survey, Reston, VA, USA, 2000.

[3] L. Decanini, C. Gavarini, and F. Mollaioli, "Some remarks on the Umbria-Marche earthquakes of 1997," *European Earthquake Engineering*, vol. 3, pp. 18–48, 2000.

[4] L. D. Decanini, D. Liberatore, L. Liberatore, and L. Sorrentino, "Preliminary report on the 2012, May 20, Emilia earthquake," vol. 1, Sapienza University of Rome, Rome, Italy, 2012.

[5] K. Chansawat, T. Potisuk, T. H. Miller, S. C. Yim, and D. I. Kachlakev, "FE models of GFRP and CFRP strengthening of reinforced concrete beams," *Advances in Civil Engineering*, vol. 2009, Article ID 152196, 13 pages, 2009.

[6] A. M. H. Kadhim, H. A. Numan, and M. Özakça, "Flexural strengthening and rehabilitation of reinforced concrete beam using BFRP composites: finite element approach," *Advances in Civil Engineering*, vol. 2019, Article ID 4981750, 17 pages, 2019.

[7] N. Askandar and A. Mahmood, "Comparative investigation on torsional behaviour of RC beam strengthened with CFRP fabric wrapping and near-surface mounted (NSM) steel bar," *Advances in Civil Engineering*, vol. 2019, Article ID 9061703, 15 pages, 2019.

[8] L. Lam and J. G. Teng, "Design-oriented stress-strain model for FRP-confined concrete," *Construction and Building Materials*, vol. 17, no. 6-7, pp. 471–489, 2003.

[9] Y.-Y. Wei and Y.-F. Wu, "Unified stress-strain model of concrete for FRP-confined columns," *Construction and Building Materials*, vol. 26, no. 1, pp. 381–392, 2012.

[10] M. Samaan, A. Mirmiran, and M. Shahawy, "Model of concrete confined by fiber composites," *Journal of Structural Engineering*, vol. 124, no. 9, pp. 1025–1031, 1998.

[11] C. Pellegrino and C. Modena, "Analytical model for FRP confinement of concrete columns with and without internal steel reinforcement," *Journal of Composites for Construction*, vol. 14, no. 6, pp. 693–705, 2010.

[12] M. H. Harajli and A. A. Rteil, "Effect of confinement using fiber-reinforced polymer or fiber-reinforced concrete on seismic performance of gravity load-designed columns," *ACI Structural Journal*, vol. 101, no. 1, pp. 47–56, 2004.

[13] S. A. Sheikh and G. Yau, "Seismic behavior of concrete columns confined with steel and fiber-reinforced polymers," *ACI Structural Journal*, vol. 99, no. 1, pp. 72–80, 2002.

[14] Y. Li, M.-F. Xie, and J.-B. Liu, "Experimental study on the seismic behaviour of reinforced concrete bridge piers strengthened by BFRP sheets," *Advances in Civil Engineering*, vol. 2019, Article ID 4169421, 11 pages, 2019.

[15] A. Rahai and H. Akbarpour, "Experimental investigation on rectangular RC columns strengthened with CFRP composites under axial load and biaxial bending," *Composite Structures*, vol. 108, pp. 538–546, 2014.

[16] A. Balsamo, A. Colombo, G. Manfredi, P. Negro, and A. Prota, "Seismic behavior of a full-scale RC frame repaired using CFRP laminates," *Engineering Structures*, vol. 27, no. 5, pp. 769–780, 2005.

[17] M. D. Ludovico, A. Prota, G. Manfredi, and E. Cosenza, "Seismic strengthening of an under-designed RC structure

with FRP," *Earthquake Engineering & Structural Dynamics*, vol. 37, no. 1, pp. 141–162, 2008.

[18] M. D. Ludovico, G. Manfredi, E. Mola, P. Negro, and A. Prota, "Seismic behavior of a full-scale RC structure retrofitted using GFRP laminates," *Journal of Structural Engineering*, vol. 134, no. 5, pp. 810–821, 2008.

[19] V. V. Cao and H. R. Ronagh, "Reducing the seismic damage of reinforced concrete frames using FRP confinement," *Composite Structures*, vol. 118, pp. 403–415, 2014.

[20] R. Garcia, I. Hajirasouliha, and K. Pilakoutas, "Seismic behaviour of deficient RC frames strengthened with CFRP composites," *Engineering Structures*, vol. 32, no. 10, pp. 3075–3085, 2010.

[21] D. Y. Wang, Z. Y. Wang, H. Li, and S. T. Smith, "Shaking table test of large scale nonductile RC frames retrofitted with FRP composites," in *Proceedings of the Fourth Asia-Pacific Conference on FRP in Structures (APFIS 2013)*, Melbourne, Vic, Australia, December 2013.

[22] A. Mortezaei, H. R. Ronagh, and A. Kheyroddin, "Seismic evaluation of FRP strengthened RC buildings subjected to near-fault ground motions having fling step," *Composite Structures*, vol. 92, no. 5, pp. 1200–1211, 2010.

[23] A. Eslami and H. R. Ronagh, "Effect of FRP wrapping in seismic performance of RC buildings with and without special detailing—a case study," *Composites Part B: Engineering*, vol. 45, no. 1, pp. 1265–1274, 2013.

[24] C.-H. Zhai, W.-P. Wen, Z. Chen, S. Li, and L.-L. Xie, "Damage spectra for the mainshock-aftershock sequence-type ground motions," *Soil Dynamics and Earthquake Engineering*, vol. 45, pp. 1–12, 2013.

[25] A. Moustafa and I. Takewaki, "Response of nonlinear single-degree-of-freedom structures to random acceleration sequences," *Engineering Structures*, vol. 33, no. 4, pp. 1251–1258, 2011.

[26] K. Goda, "Nonlinear response potential of mainshock-aftershock sequences from Japanese earthquakes," *Bulletin of the Seismological Society of America*, vol. 102, no. 5, pp. 2139–2156, 2012.

[27] S. Yaghmaei-Sabegh and J. Ruiz-García, "Nonlinear response analysis of SDOF systems subjected to doublet earthquake ground motions: a case study on 2012 Varzaghan-Ahar events," *Engineering Structures*, vol. 110, pp. 281–292, 2016.

[28] C. Durucan and A. R. Durucan, "A_p/V_p specific inelastic displacement ratio for the seismic response estimation of SDOF structures subjected to sequential near fault pulse type ground motion records," *Soil Dynamics and Earthquake Engineering*, vol. 89, pp. 163–170, 2016.

[29] G. D. Hatzigeorgiou and D. E. Beskos, "Inelastic displacement ratios for SDOF structures subjected to repeated earthquakes," *Engineering Structures*, vol. 31, no. 11, pp. 2744–2755, 2009.

[30] K. Goda and C. A. Taylor, "Effects of aftershocks on peak ductility demand due to strong ground motion records from shallow crustal earthquakes," *Earthquake Engineering & Structural Dynamics*, vol. 41, no. 15, pp. a–n, 2012.

[31] G. D. Hatzigeorgiou, "Ductility demand spectra for multiple near- and far-fault earthquakes," *Soil Dynamics and Earthquake Engineering*, vol. 30, no. 4, pp. 170–183, 2010.

[32] C. Amadio, M. Fragiacomo, and S. Rajgelj, "The effects of repeated earthquake ground motions on the non-linear response of SDOF systems," *Earthquake Engineering & Structural Dynamics*, vol. 32, no. 2, pp. 291–308, 2003.

[33] G. D. Hatzigeorgiou, "Behavior factors for nonlinear structures subjected to multiple near-fault earthquakes," *Computers & Structures*, vol. 88, no. 5-6, pp. 309–321, 2010.

[34] C.-H. Zhai, W.-P. Wen, S. Li, and L.-L. Xie, "The ductility-based strength reduction factor for the mainshock-aftershock sequence-type ground motions," *Bulletin of Earthquake Engineering*, vol. 13, no. 10, pp. 2893–2914, 2015.

[35] A. Faisal, T. A. Majid, and G. D. Hatzigeorgiou, "Investigation of story ductility demands of inelastic concrete frames subjected to repeated earthquakes," *Soil Dynamics and Earthquake Engineering*, vol. 44, pp. 42–53, 2013.

[36] F. Hosseinpour and A. E. Abdelnaby, "Fragility curves for RC frames under multiple earthquakes," *Soil Dynamics and Earthquake Engineering*, vol. 98, pp. 222–234, 2017.

[37] R. Han, Y. Li, and J. van de Lindt, "Impact of aftershocks and uncertainties on the seismic evaluation of non-ductile reinforced concrete frame buildings," *Engineering Structures*, vol. 100, pp. 149–163, 2015.

[38] G. D. Hatzigeorgiou and A. A. Liolios, "Nonlinear behaviour of RC frames under repeated strong ground motions," *Soil Dynamics and Earthquake Engineering*, vol. 30, no. 10, pp. 1010–1025, 2010.

[39] J. Ruiz-García, M. V. Marín, and A. Terán-Gilmore, "Effect of seismic sequences in reinforced concrete frame buildings located in soft-soil sites," *Soil Dynamics and Earthquake Engineering*, vol. 63, pp. 56–68, 2014.

[40] M. Hatzivassiliou and G. D. Hatzigeorgiou, "Seismic sequence effects on three-dimensional reinforced concrete buildings," *Soil Dynamics and Earthquake Engineering*, vol. 72, pp. 77–88, 2015.

[41] F. Yang, G. Wang, and Y. Ding, "Damage demands evaluation of reinforced concrete frame structure subjected to near-fault seismic sequences," *Natural Hazards*, vol. 97, no. 2, pp. 841–860, 2019.

[42] J. Shin, J.-S. Jeon, and J. Kim, "Mainshock-aftershock response analyses of FRP-jacketed columns in existing RC building frames," *Engineering Structures*, vol. 165, pp. 315–330, 2018.

[43] G. P. Mavroeidis and A. Papageorgiou, "A mathematical representation of near-fault ground motions," *Bulletin of the Seismological Society of America*, vol. 93, no. 3, pp. 1099–1131, 2003.

[44] A. Moustafa and I. Takewaki, "Characterization and modeling of near-fault pulse-like strong ground motion via damage-based critical excitation method," *Structural Engineering and Mechanics*, vol. 34, no. 6, pp. 755–778, 2010.

[45] E. Kalkan and S. K. Kunnath, "Effects of fling step and forward directivity on seismic response of buildings," *Earthquake Spectra*, vol. 22, no. 2, pp. 367–390, 2006.

[46] V. V. Bertero, S. A. Mahin, and R. A. Herrera, "Aseismic design implications of near-fault san fernando earthquake records," *Earthquake Engineering & Structural Dynamics*, vol. 6, no. 1, pp. 31–42, 1978.

[47] L.-Y. Lu and G.-L. Lin, "Improvement of near-fault seismic isolation using a resettable variable stiffness damper," *Engineering Structures*, vol. 31, no. 9, pp. 2097–2114, 2009.

[48] K. Galal and M. Naimi, "Effect of soil conditions on the response of reinforced concrete tall structures to near-fault earthquakes," *The Structural Design of Tall and Special Buildings*, vol. 17, no. 3, pp. 541–562, 2008.

[49] S. W. Park, H. Ghasemi, J. Shen, P. G. Somerville, W. P. Yen, and M. Yashinsky, "Simulation of the seismic performance of the bolu viaduct subjected to near-fault ground motions,"

Earthquake Engineering & Structural Dynamics, vol. 33, no. 13, pp. 1249–1270, 2004.

[50] K. Galal and A. Ghobarah, "Effect of near-fault earthquakes on North American nuclear design spectra," *Nuclear Engineering and Design*, vol. 236, no. 18, pp. 1928–1936, 2006.

[51] J. W. Baker, "Quantitative classification of near-fault ground motions using wavelet analysis," *Bulletin of the Seismological Society of America*, vol. 97, no. 5, pp. 1486–1501, 2007.

[52] F. Mollaioli, S. Bruno, L. D. Decanini, and G. F. Panza, "Characterization of the dynamic response of structures to damaging pulse-type near-fault ground motions," *Meccanica*, vol. 41, no. 1, pp. 23–46, 2006.

[53] S. Krishnan, "Case studies of damage to 19-storey irregular steel moment-frame buildings under near-source ground motion," *Earthquake Engineering & Structural Dynamics*, vol. 36, no. 7, pp. 861–885, 2007.

[54] G. Manfredi, M. Polese, and E. Cosenza, "Cumulative demand of the earthquake ground motions in the near source," *Earthquake Engineering & Structural Dynamics*, vol. 32, no. 12, pp. 1853–1865, 2003.

[55] H. Choi, M. S. Saiidi, P. Somerville, and S. El-Azazy, "Experimental study of reinforced concrete bridge columns subjected to near-fault ground motions," *ACI Structural Journal*, vol. 107, no. 1, pp. 3–12, 2010.

[56] K. C. Tsai, C. P. Hsiao, and M. Bruneau, "Overview of building damages in 921 Chi-Chi earthquake," *Earthquake Engineering and Engineering Seismology*, vol. 2, no. 1, pp. 93–108, 2000.

[57] V. V. Cao, H. R. Ronagh, and H. Baji, "Seismic risk assessment of deficient reinforced concrete frames in near-fault regions," *Advances in Concrete Construction*, vol. 2, no. 4, pp. 261–280, 2014.

[58] W.-I. Liao, C.-H. Loh, and S. Wan, "Earthquake responses of RC moment frames subjected to near-fault ground motions," *The Structural Design of Tall Buildings*, vol. 10, no. 3, pp. 219–229, 2001.

[59] E. Yüksel and M. Sürmeli, "Failure analysis of one-story precast structures for near-fault and far-fault strong ground motions," *Bulletin of Earthquake Engineering*, vol. 8, no. 4, pp. 937–953, 2010.

[60] F. Mazza and A. Vulcano, "Nonlinear dynamic response of r.c. framed structures subjected to near-fault ground motions," *Bulletin of Earthquake Engineering*, vol. 8, no. 6, pp. 1331–1350, 2010.

[61] V. V. Cao, "Characterization of near-fault effects on potential cumulative damage of reinforced concrete bridge piers," *International Journal of Civil Engineering*, vol. 17, no. 10, pp. 1063–1618, 2019.

[62] A. Furtado, H. Rodrigues, H. Varum, and A. Arêde, "Mainshock-aftershock damage assessment of infilled RC structures," *Engineering Structures*, vol. 175, pp. 645–660, 2018.

[63] L. Xie, J. Wu, Q. Huang, and C. Tong, "Analysis of the seismic demand of high-performance buckling-restrained braces under a strong earthquake and its aftershocks," *Advances in Civil Engineering*, vol. 2019, Article ID 1482736, 14 pages, 2019.

[64] ICBO, "Uniform building code," in *Proceedings of the International Conference of Building Officials*, Whittier, California, 1997.

[65] PEER, "PEER ground motion database," 2019, https://ngawest2.berkeley.edu/site.

[66] Y. Li, R. Song, and J. W. V. D. Lindt, "Collapse fragility of steel structures subjected to earthquake mainshock-aftershock sequences," *Journal of Structural Engineering*, vol. 140, no. 12, Article ID 04014095, 2014.

[67] Q. Li and B. R. Ellingwood, "Performance evaluation and damage assessment of steel frame buildings under main shock-aftershock earthquake sequences," *Earthquake Engineering & Structural Dynamics*, vol. 36, no. 3, pp. 405–427, 2007.

[68] K. Morfidis and K. Kostinakis, "The role of masonry infills on the damage response of R/C buildings subjected to seismic sequences," *Engineering Structures*, vol. 131, pp. 459–476, 2017.

[69] J. Ruiz-García, "Mainshock-aftershock ground motion features and their influence in building's seismic response," *Journal of Earthquake Engineering*, vol. 16, no. 5, pp. 719–737, 2012.

[70] J. Ruiz-García and J. C. Negrete-Manriquez, "Evaluation of drift demands in existing steel frames under as-recorded far-field and near-fault mainshock-aftershock seismic sequences," *Engineering Structures*, vol. 33, no. 2, pp. 621–634, 2011.

[71] A. Keiiti, "Asperities, barriers, characteristic earthquakes and strong motion prediction," *Journal of Geophysical Research: Solid Earth*, vol. 89, no. B7, pp. 5867–5872, 1984.

[72] M. Båth, "Lateral inhomogeneities of the upper mantle," *Tectonophysics*, vol. 2, no. 6, pp. 483–514, 1965.

[73] R. Shcherbakov, "A modified form of bath's law," *Bulletin of the Seismological Society of America*, vol. 94, no. 5, pp. 1968–1975, 2004.

[74] B. Gutenberg and C. F. Richter, "Frequency of earthquakes in California," *Bulletin of the Seismological Society of America*, vol. 34, no. 4, pp. 185–188, 1944.

[75] R. Gutenberg and C. Ritcher, *Seismicity of the Earth and Associated Phenomena*, Princeton University Press, Princeton, NJ, USA, 2nd edition, 1954.

[76] K. R. Felzer, T. W. Becker, R. E. Abercrombie, G. Ekström, and J. R. Rice, "Triggering of the 1999 MW 7.1 hector mine earthquake by aftershocks of the 1992 MW 7.3 landers earthquake," *Journal of Geophysical Research: Solid Earth*, vol. 107, no. B9, pp. ESE 6-1, 2002.

[77] M. Tahir, J. R. Grasso, and D. Amorèse, "The largest aftershock: how strong, how far away, how delayed?" *Geophysical Research Letters*, vol. 39, no. 4, 2012.

[78] K.-C. Chen and J.-H. Wang, "Correlations between the mainshock and the largest aftershock for Taiwan earthquakes," *Pure and Applied Geophysics*, vol. 169, no. 7, pp. 1217–1229, 2012.

[79] V. V. Cao and S. Q. Pham, "Comparison of CFRP and GFRP wraps on reducing seismic damage of deficient reinforced concrete structures," *International Journal of Civil Engineering*, vol. 17, no. 11, pp. 1667–1681, 2019.

[80] ASCE, *Prestandard and Commentary for the Seismic Rehabilitation of Buildings*, Federal Emergency Management Agency, Washington, DC, USA, 2000.

[81] ACI, *Building Code Requirements for Structural Concrete (ACI 318M-08) and Commentary*, American Concrete Institute, Farmington Hills, MI, USA, 2008.

[82] A. D. Luca, F. Nardone, F. Matta, A. Nanni, G. P. Lignola, and A. Prota, "Structural evaluation of full-scale FRP-confined reinforced concrete columns," *Journal of Composites for Construction*, vol. 15, no. 1, pp. 112–123, 2011.

[83] L.-M. Wang and Y.-F. Wu, "Effect of corner radius on the performance of CFRP-confined square concrete columns: test," *Engineering Structures*, vol. 30, no. 2, pp. 493–505, 2008.

[84] R. Park, M. J. N. Priestley, and W. D. Gill, "Ductility of square-confined concrete columns," *Journal of the Structural Division*, vol. 108, no. 4, pp. 929–950, 1982.
[85] T. Paulay and M. J. N. Priestley, *Seismic Design of Reinforced Concrete and Masonry Buildings*, John Wiley & Sons, Newyork, NY, USA, 1992.
[86] S. A. Sheikh and S. S. Khoury, "Confined concrete columns with stubs," *ACI Structural Journal*, vol. 90, no. 4, pp. 414–431, 1993.
[87] Computers and Structures Inc, *SAP2000 Version 19.2.0*, Computers and Structures Inc., Berkeley, CA, USA, 2017.
[88] T. Takeda, M. A. Sozen, and N. N. Nielsen, "Reinforced concrete response to simulated earthquakes," *Journal of the Structural Division*, vol. 96, no. 12, pp. 2557–2573, 1970.
[89] L. Lam and J. G. Teng, "Design-oriented stress-strain model for FRP-confined concrete in rectangular columns," *Journal of Reinforced Plastics and Composites*, vol. 22, no. 13, pp. 1149–1186, 2003.
[90] M. H. Harajli, E. Hantouche, and K. Soudki, "Stress-strain model for fiber-reinforced polymer jacketed concrete columns," *ACI Structural Journal*, vol. 103, no. 5, pp. 672–682, 2006.
[91] G. Wu, Z. S. Wu, and Z. T. Lü, "Design-oriented stress-strain model for concrete prisms confined with FRP composites," *Construction and Building Materials*, vol. 21, no. 5, pp. 1107–1121, 2007.
[92] M. N. Youssef, M. Q. Feng, and A. S. Mosallam, "Stress-strain model for concrete confined by FRP composites," *Composites Part B: Engineering*, vol. 38, no. 5-6, pp. 614–628, 2007.
[93] S. Rocca, N. Galati, and A. Nanni, "Interaction diagram methodology for design of FRP-confined reinforced concrete columns," *Construction and Building Materials*, vol. 23, no. 4, pp. 1508–1520, 2009.
[94] H. Baji, "Calibration of the FRP resistance reduction factor for FRP-confined reinforced concrete building columns," *Journal of Composites for Construction*, vol. 21, no. 3, Article ID 04016107, 2017.
[95] T. Chaudat, C. Garnier, S. Cvejic, S. Poupin, M. Le Corre, and M. Mahe, "ECOLEADER project no. 2: seismic tests on a reinforced concrete bare frame with FRP retrofitting," Tests Report. SEMT/EMSI/RT/05-006/A, CEA, Saclay, France, 2005.
[96] V. V. Cao, H. R. Ronagh, M. Ashraf, and H. Baji, "A new damage index for reinforced concrete structures," *Earthquakes and Structures*, vol. 6, no. 6, pp. 581–609, 2014.